OPTIMIZING ROBOTIC AQUATIC LOCOMOTION

WENDY SAINTVAL

BARRY UNIVERSITY

Saintval, Wendy (B.S., Mathematics)

Optimizing Robotic Aquatic Locomotion April/2001

Abstract of tentative senior thesis at Barry University. Thesis supervised by Professor Mysore S. Jagadish.

Number of pages in text 15

Carangiform (tuna-like) swimming is effective in producing forward thrust through counter-rotating vortices left in the wake. B. Ahlborn *et al.* (1997) mimicked carangiform motions with a computer–controlled fishtail simulation apparatus. Ahlborn *et al.* states two claims: (i) fish hide their "footprints" through the destruction of these vortices, which increases efficiency and (ii) thrust force of his vortex-producing robot is derived by $F_x = (2/\pi)K\rho hA^3f^2$. K is a water entrainment constant of 40, ρ is the density of water, h is the submerged height of the tailfin, A is the deflection amplitude, and f is the frequency. While the peduncle's deflection amplitude was held constant, we swam our carangiform-swimming robot using 160 unique motions (gaits) to obtain values of efficiency and velocity at four distinct frequencies, ten distinct phase angles, and four distinct tailfin amplitudes. Maximum values of efficiency and velocity were found on 3-D surfaces. Our experimental thrust force was estimated by creating a function of drag forces at different steady-state velocities. When using Ahlborn *et al.*'s equation, our thrust force appeared to be proportional to a square root function of the frequency. Under certain constraints, we determined optimal thrust and efficiency, which yields the best gait at 40P80W20. Understanding these relationships allows us to control and predict the efficiency, velocity, and thrust force of our robot within certain parameters.

Acknowledgments

From the California Institute of Technology, I would like to thank Dr. Joel W. Burdick and Richard Mason for their undivided attention, guidance, and passion for research. I appreciate the SURF/MURF Program for providing a unique summer research experience. From Barry University, I would like to thank Dr. Mysore S. Jagadish, Dr. Flona Redway, and Sr. John Karen Frei, O.P. for playing the role of guardian, sacrificing their time, and sharing their wisdom. I am also thankful of the Department of Mathematics and Computer Science for challenging my intellect and encouraging my efforts. I appreciate the continued support, advice, and love given freely and fully by my never-ending source of strength (Pappi), heart (Mummi), soul (Kentey), charm (Walter), sense (Hophni), and youthful joy (Egen). I would like to give another loving thank you to my friends for being cool and smart; I send humble praises to our omniscient Creator. Funding has been provided by the NSF Cooperative Agreement No. EEC-9402726 and the NIH-NIGMS MARC U*STAR GM0821-17.

Chapter 1, Introduction

Fish are excellent, efficient swimmers. By adding momentum to the water and shedding counter-rotating vortices in the wake, a swimming fish can produce forward thrust through undulating motions of its body and/or tail (Ahlborn *et al.* 1997, Muller *et al.* 1997). Five of the various locomotion modes are anguilliform (eel-like), sub-carangiform (i.e. trout), carangiform (i.e. mullet), thunniform (i.e. bluefin tuna), and ostraciiform (oscillatory).

For several decades, mechanical engineers have attempted to reproduce the motions of this animal with robots. These scientists have attempted to mechanically replicate the relative quietness, high maneuverability, high adaptability, and high efficiency that fish have demonstrated for many years. Since there is no handbook on building such robots, many of the ideas are innovative and creative. For instance, the Charles Stark Draper Laboratory and the Massachusetts Institute of Technology (MIT) have engineered robots to swim like fish. Draper Laboratory created the Vorticity Control Unmanned Underwater Vehicle (VCUUV); MIT produced RoboTuna. Both robots attempt free-swimming.

One of the main difficulties in doing this successfully is that fish are very complex. For a free-swimming fish, the degrees of freedom are found in the pitch, roll, spin, lateral, longitudinal, and vertical displacements. This does not take into account the many other degrees created along the body, like bending and twisting. Therefore, engineers have had to make innovative robots and use mathematical models to get the best performance from their designs. The use of mathematics has been an essential tool to these pioneers.

At the California Institute of Technology, we studied issues in fluid mechanics, nonlinear control, and sensing that are necessary for the development of a self-propelled robot. In our

laboratory, our robot “fish” could swim in both carangiform and thunniform swimming modes. Finding optimal motions at the different levels of efficiency, velocity, and thrust provides an understanding of the performance and control of the robot. For a given gait input, we should be able to predict the values of velocity, efficiency, and thrust forces.

Multiobjective Optimization (MO), also known as multicriteria and vector optimization, can be used to find the best tradeoff of values between two interdependent objects. Usually, improvement in one object's value would cause the other object to lose value, and vice versa. In our case, we wanted to find the “best” gait by optimizing the thrust and efficiency ratio for our robot.

Chapter 2, Background Information

Various studies, from such fields as biology, mathematics, and engineering, are useful in studying how fish swim, naturally and mechanically. Marine biologists have studied vortex shedding in the wake and the interaction between the water and the fish body (Muller *et al.* 1997). They have approximated the motion of a mullet to be sinusoidal (Muller *et al.* 1997). M. J. Lighthill (1970) offers a preliminary quantitative analysis of how a series of modifications to that basic undulatory mode, found in vertebrates (and especially fish), tends to improve speed and hydromechanical efficiency. He states that the carangiform mode is advantageous from the point of view of propulsive efficiency. Ahlborn *et al. (*1997) claimed that fish hide their "footprints" through the destruction of these vortices, which increases efficiency. Carangiform locomotion is evident when the final third to half of the body is undulating while the remainder is fairly rigid. Carangiform-like swimming is effective in creating counter-rotating vortices, whirling masses of water within a limited area (Fig. 1).

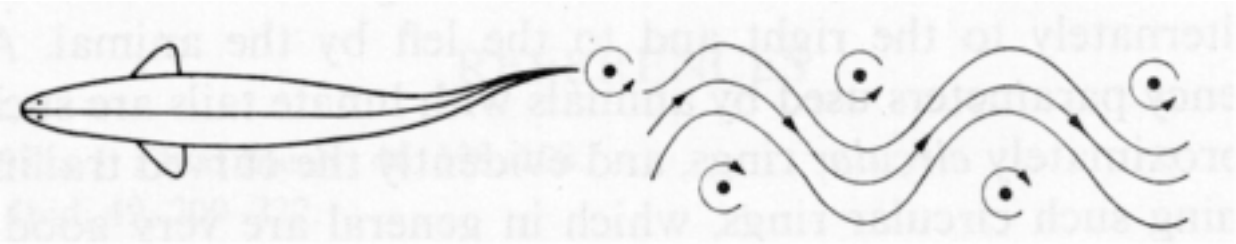

Fig. 1. Thrust production in the wake.

The equation for thrust force based on experiments with a vortex-shedding apparatus (Ahlborn *et al.* 1990, Ahlborn *et al.* 1997) follows:

$$F_x = \frac{2}{\pi} K \rho h A^3 f^2 \qquad (1)$$

Ahlborn *et al.* computer-controlled apparatus has a tail that moves in premeditated paths and focused mainly on half-flips. It created a vortex with the first tail flip (Ahlborn *et al.* 1997). Then inverted the vortex on the return stroke (Ahlborn *et al.* 1997). Equation one describes the thrust force produced along the direction of motion. Shapiro (1961) used drag experiments as a vehicle for discussing the fundamentals of fluid dynamics.

Mathematicians used optimization for various applications. According to Eschenauer *et al.* (1986), Gottfried W. Leibniz and Leonhard Euler used infinitesimal calculus to find the extreme values of functions. This made it possible for pioneers to study various new fields of mechanics (Eschenauer *et al.* 1986). For example, Bernoulli and D. Bernoulli used optimization on isoperimetric problems; Isaac Newton used the method for minimizing the resistance of a revolving body (Eschenauer *et al.* 1986). Vilfredo Pareto initially used MO in economics (Eschenauer *et al.* 1986). Using this technique can aid us in our understanding of underwater locomotion and control of our robot's performance.

The experiments were performed by swimming a computer-controlled robot, which is supported by a carriage that rolled on a pair of frictionless rails that ran parallel along the top of the aquarium (Fig. 2a). This carriage held the twin motors with motor encoders, transmission, and a Polhemus 3-space motion sensor. The Polhemus motion sensor is in a fixed position. The Polhemus 3-D detector receives and records the three-dimensional position of the sensor over time. The design specifications of the robot can be obtained on request.

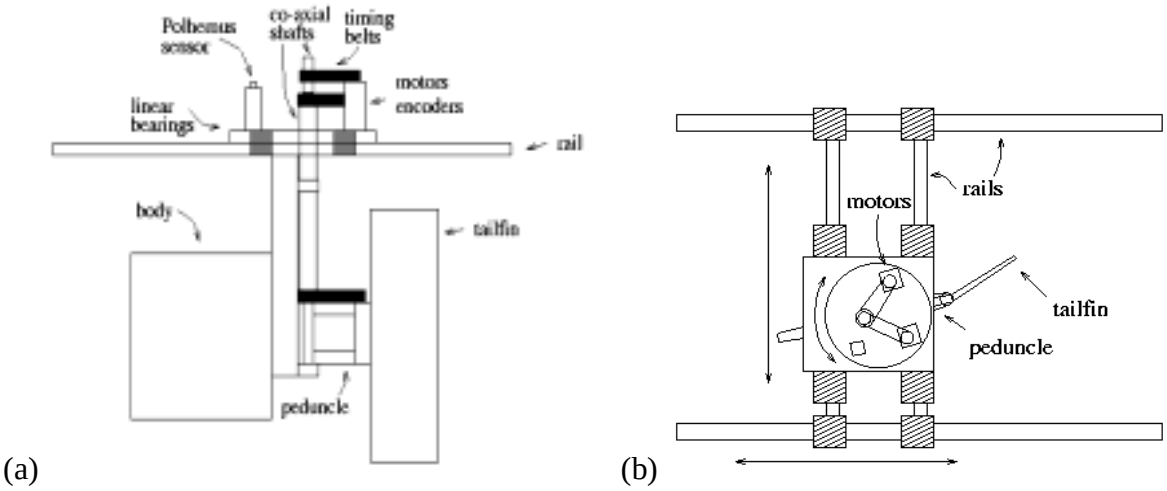

Fig. 2. (a) Side and (b) top view of robot.

To mimic carangiform motion, the three-link robot used the final third of its body to move while the rest of the body was fairly rigid. This third had two main parts called the peduncle and tailfin, which both turned independently about its respective joint in a sinusoidal manner (Fig. 3). The robot was designed to propel itself by two joint degrees of freedom for the peduncle and the tailfin. Additionally, it had one to three degrees of freedom for lateral, longitudinal and rotational motions within the plane of the water surface (Fig. 2b). For our experiment, motions were limited to three degrees of freedom at the turning at the two joints and

the forward motion. Motors encoders measure the actual angles created by each motor. These values are stored in matrices, joutp and joutt. Based on the difference between desired and actual θ values, the computer increased or decreased power sent to the motor(s).

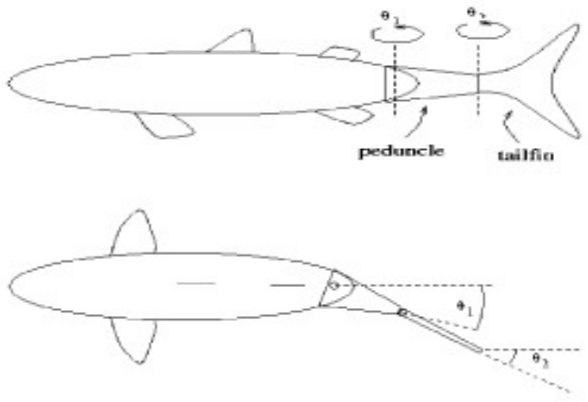

(a)

(b)

Fig. 3. (a) Side and (b) top view of three-link robotic carangiform locomotion.

The peduncle and tailfin move as a sinusoidal function of time (Fig. 4). Both joint angles, θ_1 and θ_2 --- in obvious notation, θ_p and θ_t --- are independent of each other (see Fig. 3). We have joint angles represented such that

$$\theta_p = (\omega t + \phi_p) \tag{2}$$

and

$$\theta_t = (\omega t + \phi_t). \tag{3}$$

However, we let

$$\theta_p = \omega t \tag{4}$$

and

$$\theta_t = \omega_t + \phi \tag{5}$$

with

$$\phi = (\phi_t + \phi_p), \tag{6}$$

for a single phase-difference variable. The amplitudes, A_p and A_t, were measured in encoder ticks, where 90° deflection is equivalent to 512 encoder ticks. We created unique gaits by inputting a text file with the desired parameters and using equations that follows:

$$j_p = A_p \sin(\omega t) \tag{7}$$

$$j_t = A_t \sin(\omega t + \phi). \quad (8)$$

Text files were inputted as gait names that were represented by two digits for the phase angle, followed by a "P", the frequency in tenths of radians per second, followed by a "W" for "ω," one digit for the amplitude of the peduncle, and one digit for the amplitude of the tailfin. For example, “40P20W23” commanded the robot to swim at a frequency of 2.0 radians per second with the peduncle amplitude at 2 in hundreds of encoder ticks, and the tailfin at 3 in hundreds of encoder ticks (Fig. 4).

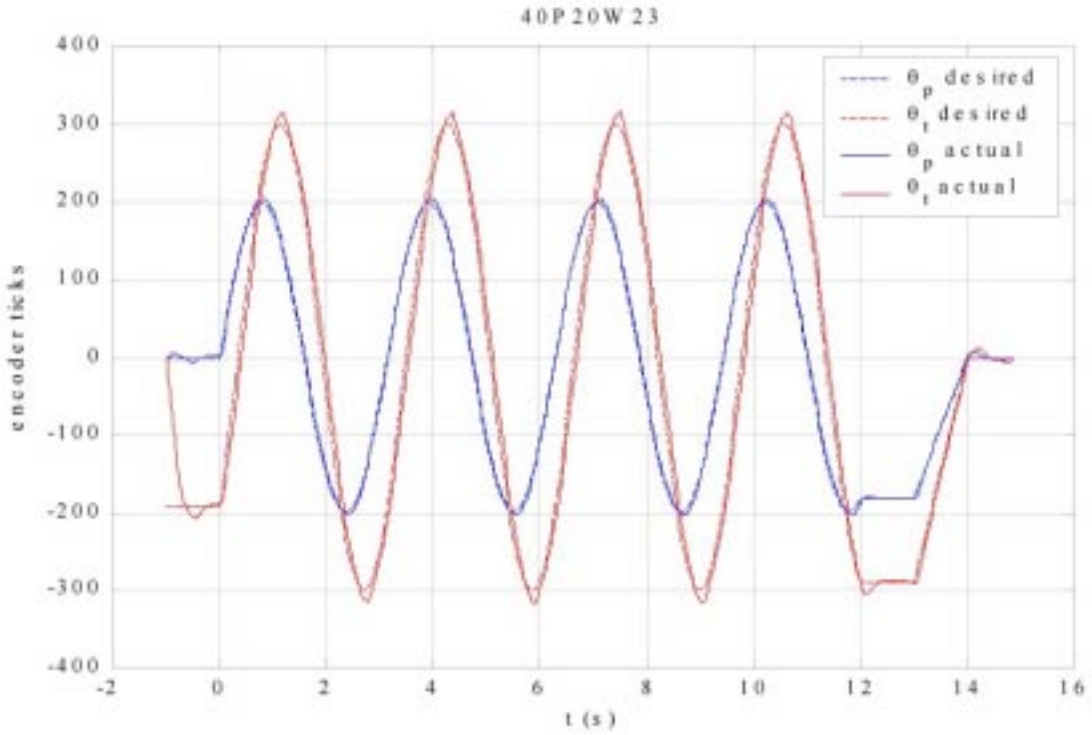

Fig. 4. Sinusoidal motion of tailfin and peduncle for 40-degree phase difference, frequency of 2.0 rad/s, peduncle’s amplitude at 200 encoder ticks, and tailfin amplitude at 300 encoder ticks.

We used our desired parameters to create a unique gait name. After we entered a gait name, the robot “swam” while a Polhemus 3-D detector received and recorded the three-dimensional position of the robot body over time. Data was obtained for 160 unique gaits for 4 distinct frequencies, 4 distinct amplitudes, and 10 distinct phase-difference angles. Values of

efficiency and velocity were derived. The frequencies were 2.0, 4.0, 6.0, and 8.0 radians per second. The amplitude values were at 0, 100, 200, and 300 encoder ticks. The phase-difference values were taken from 0° to 90° by increments of 10°.

Optimizing velocity

Position was plotted at every fiftieth of a second (Fig. 5). Elapsed time per gait ranged from 12-15 seconds. Velocity was calculated by the distance traveled over the change of time, from 0.5 to 9.5 seconds. Three-dimensional surfaces of velocity were constructed for each of the frequencies (Fig. 6-9). These surfaces illustrated the relationship between different parameters of frequency, tailfin amplitude, and phase angle.

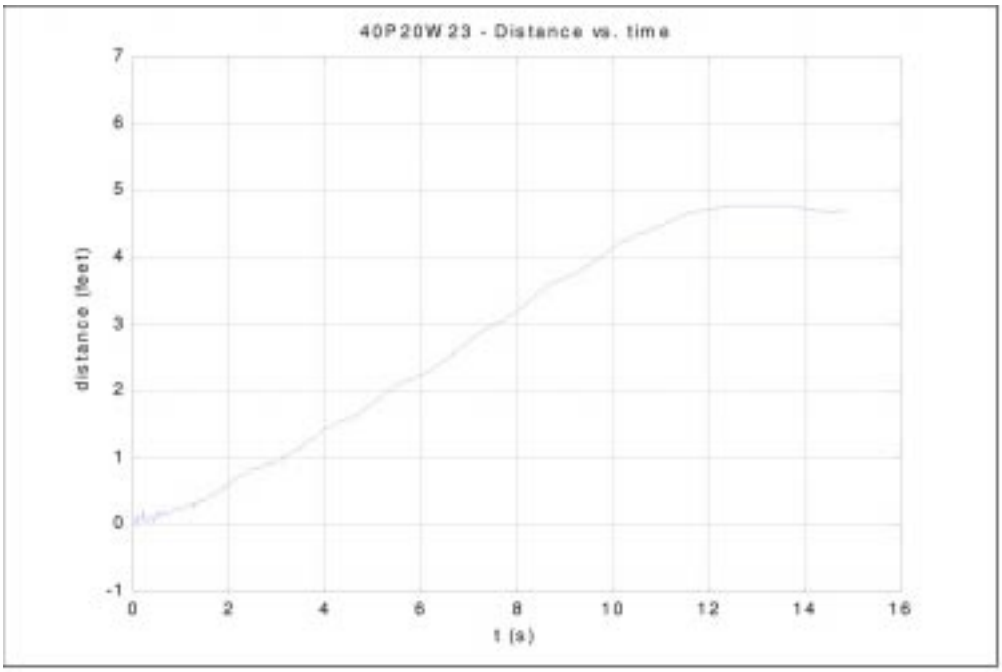

Fig. 5. Distance traveled over time.

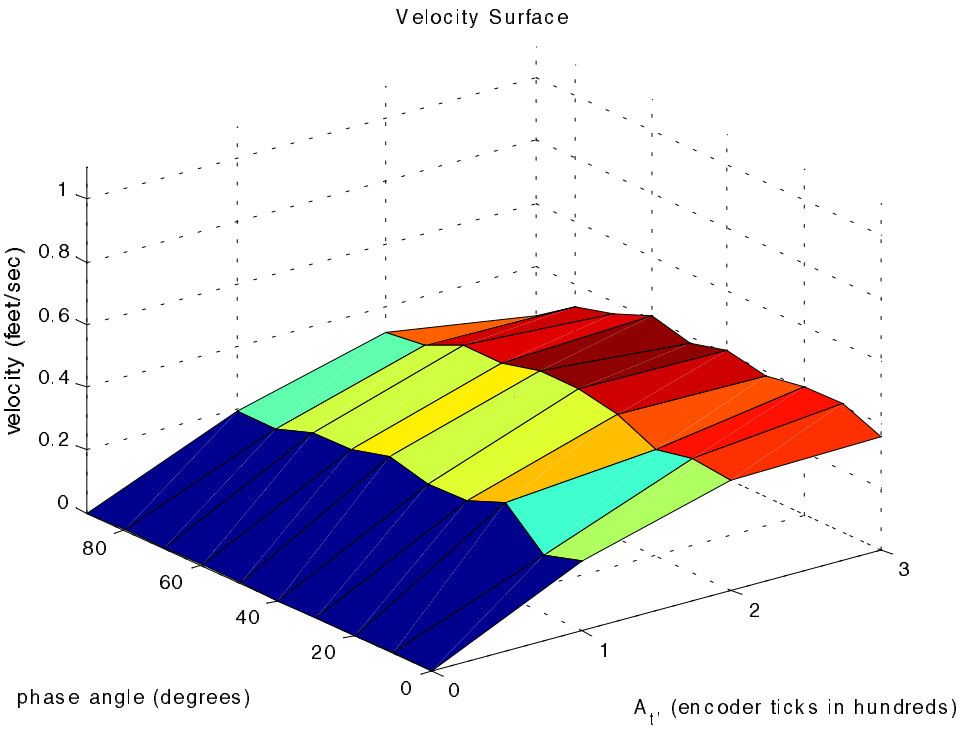

Fig. 6. Frequency is 2.0 rad/sec.

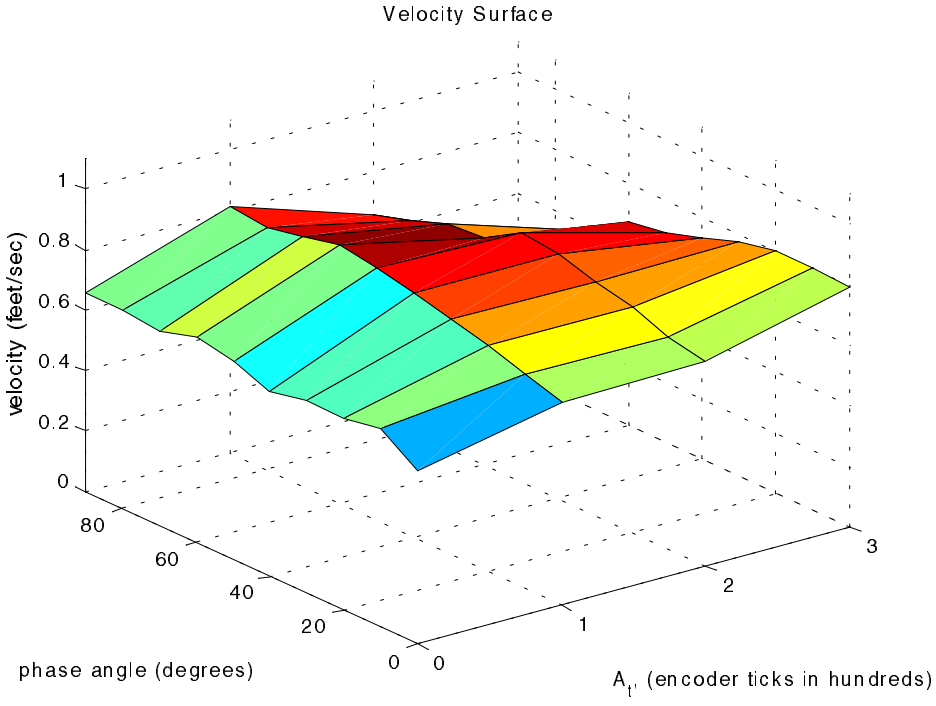

Fig. 7. Frequency is 4.0 rad/sec.

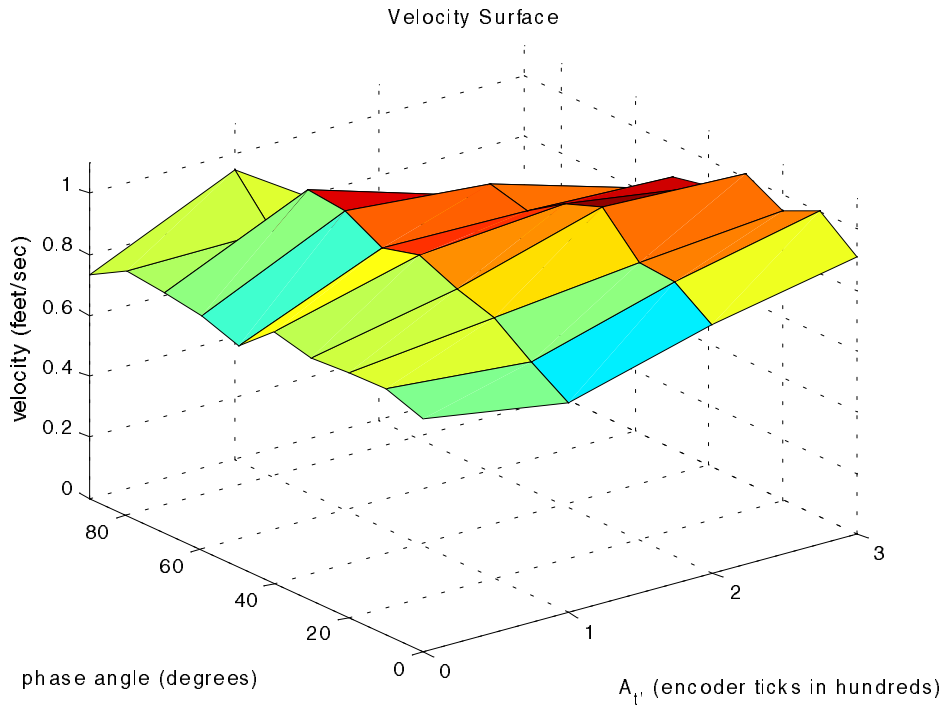

Fig. 8. Frequency is 6.0 rad/sec.

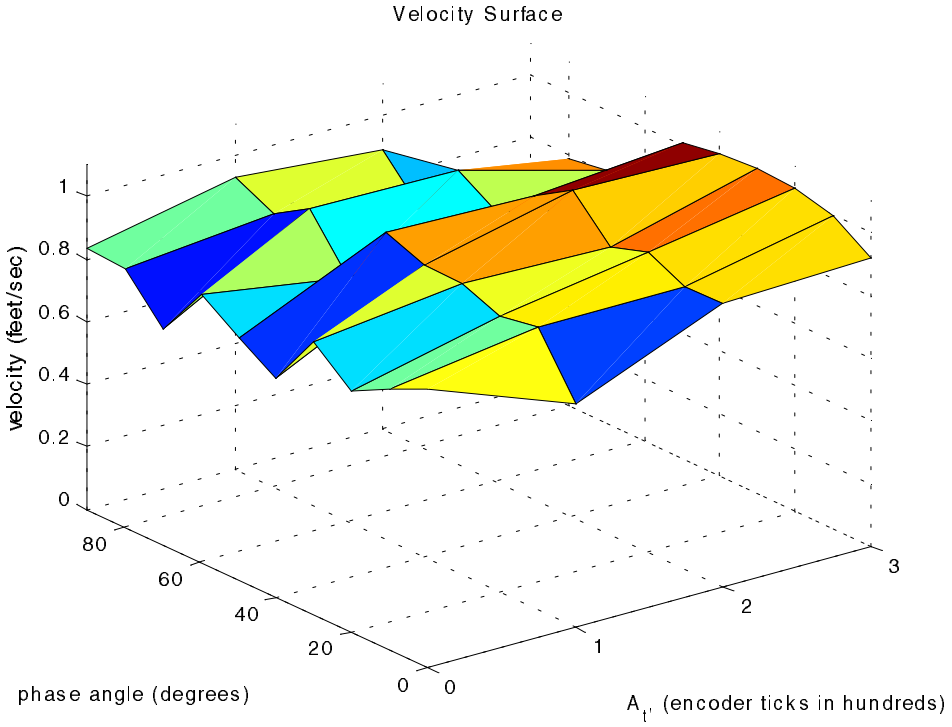

Fig. 9. Frequency is 8.0 rad/sec.

Optimizing efficiency

Relative efficiency is a function of velocity and the total power. It was calculated by dividing the total kinetic energy by the total power given to the motors during each run (Eqns. 9-11). The mass, m, of the entire robot was 34 kg (approx. 74.8 lbs). We constructed 3-D surfaces of efficiency for each of the frequencies (Fig. 10-14).

$$KE = \frac{1}{2}mv^2 \tag{9}$$

$$\text{Total power} = \text{power}_1 + \text{power}_2 \tag{10}$$

$$\text{Efficiency} = \frac{KE}{(\text{Total power})} \tag{11}$$

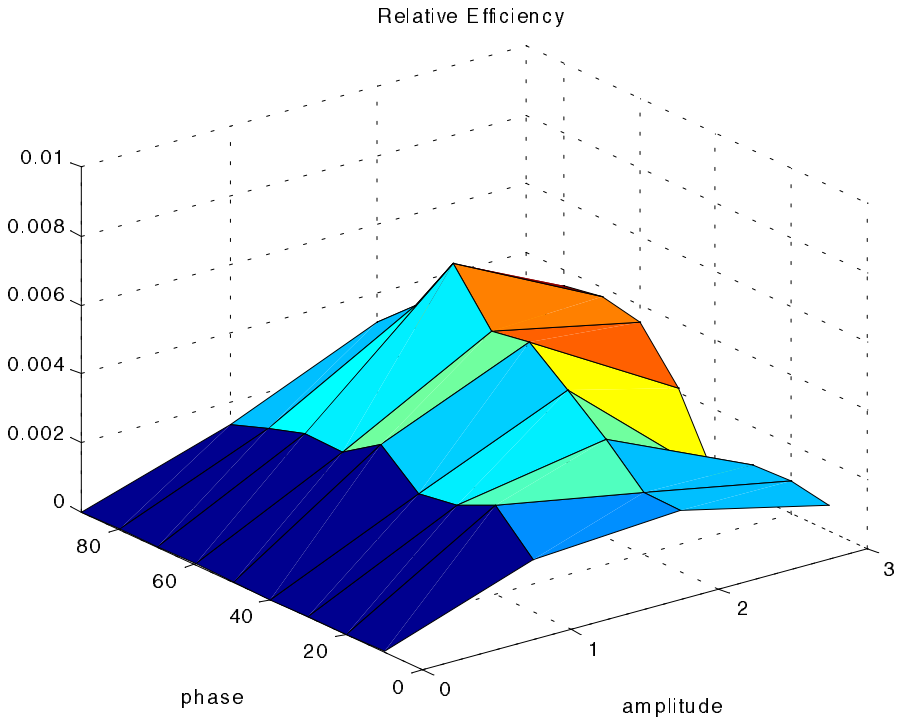

Fig. 10. Frequency is 2.0 rad/sec.

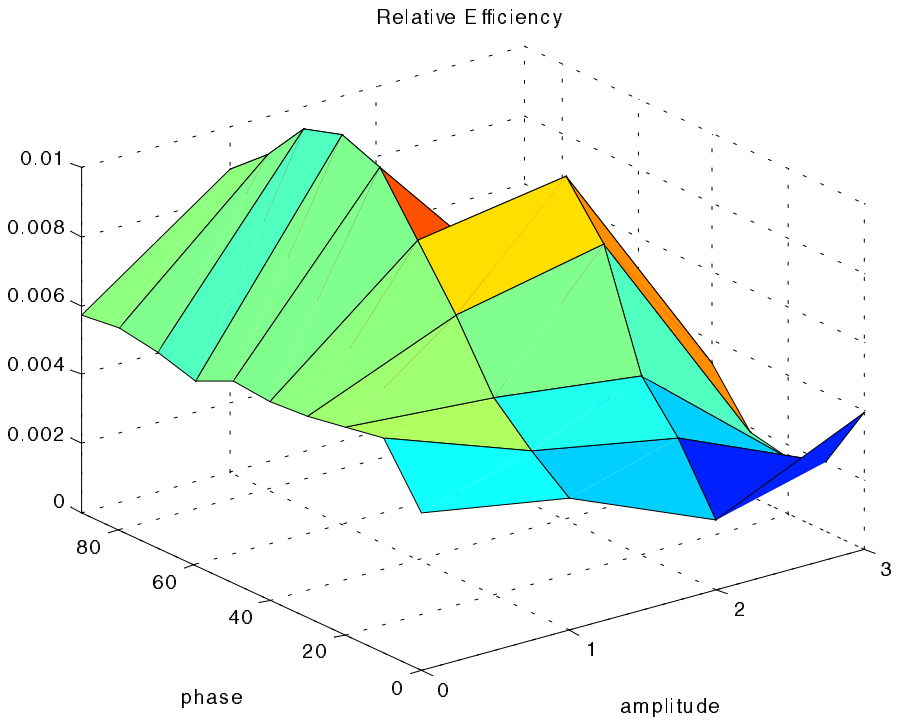

Fig. 11. Frequency is 4.0 rad/sec.

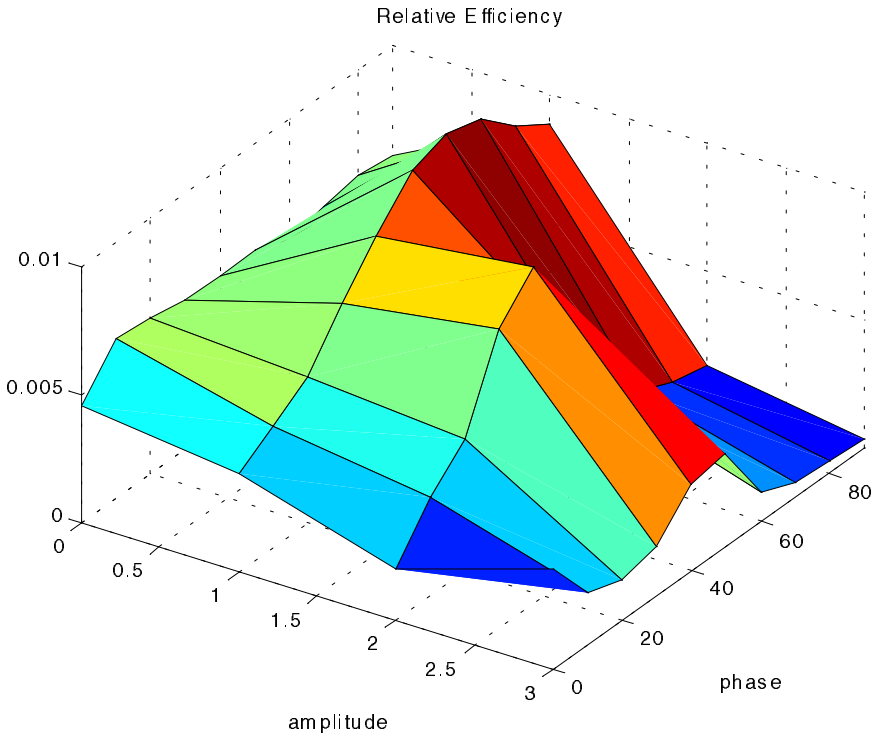

Fig. 12. Please, notice that the x and y-axes are switched from Fig. 11.

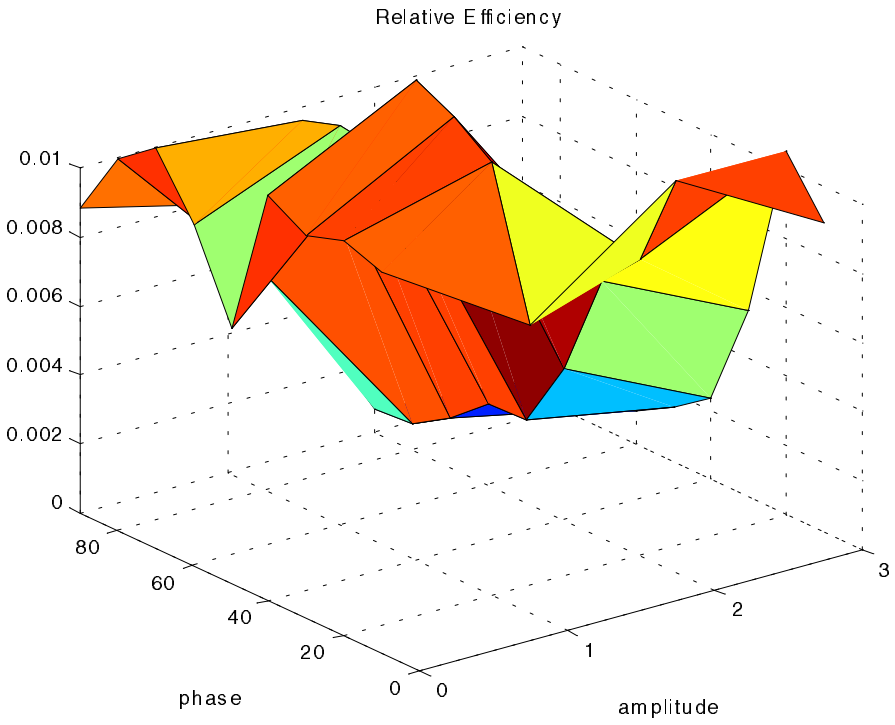

Fig. 13. Frequency is 6.0 rad/sec.

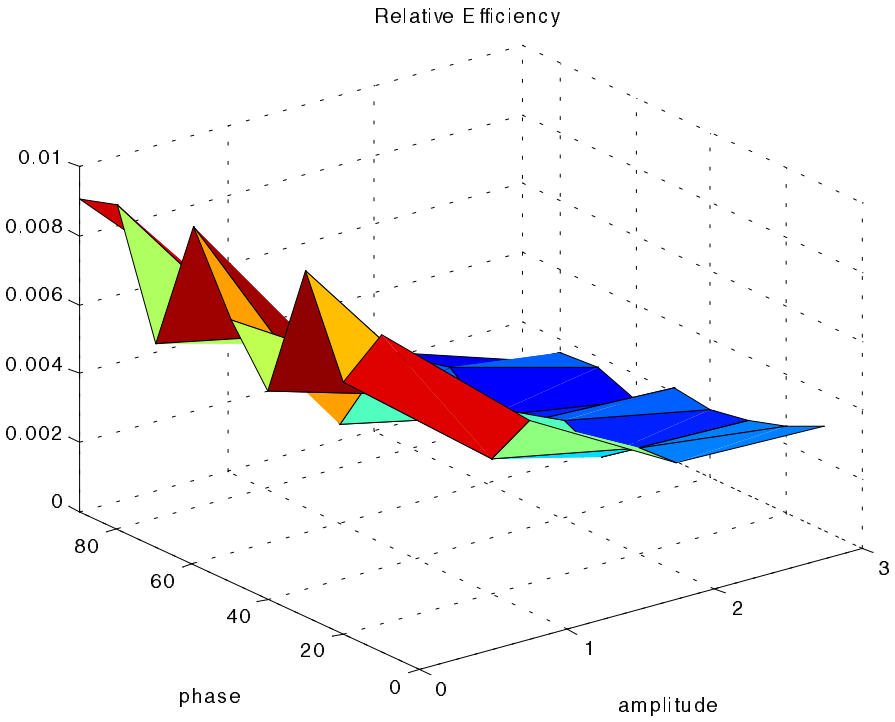

Fig. 14. Frequency is 8.0 rad/sec.

Controlling thrust

Equation 1 was analyzed. For the experimental thrust, K and ρ remained as our constants. Frequency values were 2.0, 4.0, 6.0, and 8.0 radians/second. Our submerged height, h, was 17.5 inches. Since A is the deflection amplitude of the tail tip, we converted our amplitudes values in MATLAB by using the equations that follows:

$$A = \frac{|\, hmax+hmin \,|}{2}, \tag{12}$$

where

$$hmax=max(lp*sin(\frac{joutp*2\pi}{2048})+lt*sin(\frac{joutt*2\pi}{2048})) \tag{13}$$

and

$$hmin=min(lp*sin(\frac{joutp*2\pi}{2048})+lt*sin(\frac{joutt*2\pi}{2048})) \tag{14}$$

The length of the peduncle, lp, was 0.127m (5 inches); the length of the tailfin, lt, was 0.1651m (6.5 inches). To find the experimental thrust force, we applied a constant force to the robot by tying a nylon string and tested different weights on a pulley system. As the robot moved in the forward direction, the drag force increased and acceleration decreased from its initial value of 9.8 m/s^2. It reached a steady-state velocity. At a steady-state velocity,

$$\text{Acceleration} = \frac{|\, T - D \,|}{\text{mass}} = 0, \tag{15}$$

which lead to

$$|\, T - D \,| = 0, \tag{16}$$

demonstrating that the steady state drag is equal to the steady state thrust. We used the Polhemus to obtain a steady state velocity value for each weight (constant force). Using MATLAB, a thrust force versus velocity relationship was found using the linear and quadratic polyfit. For a constant acceleration, steady-state drag measurements were plotted against steady-state velocity values (Figs. 15-16).

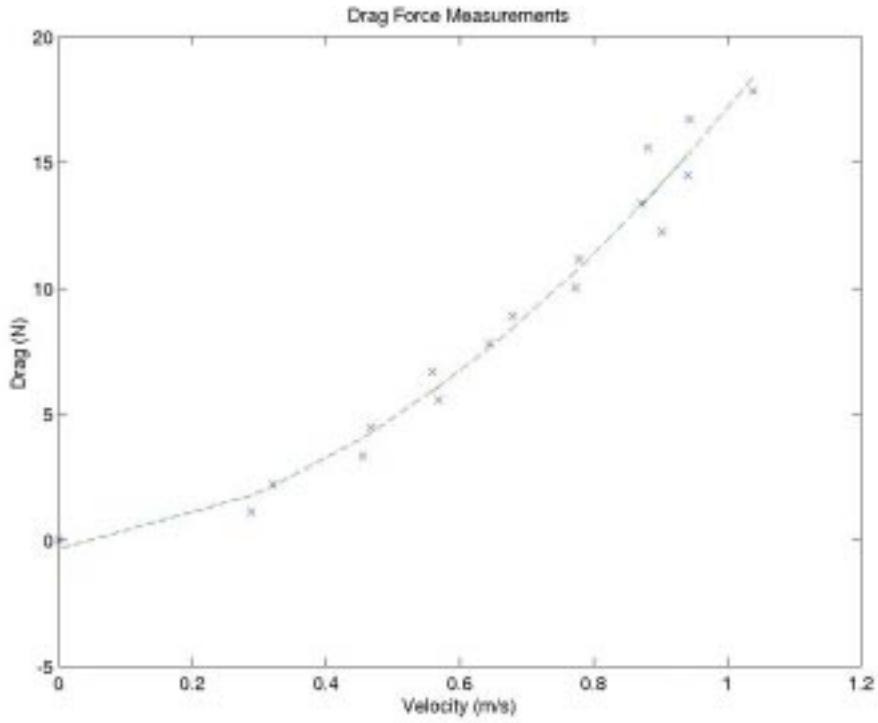

Fig. 15. Experimental steady state drag measurements with quadratic polyfit curve.

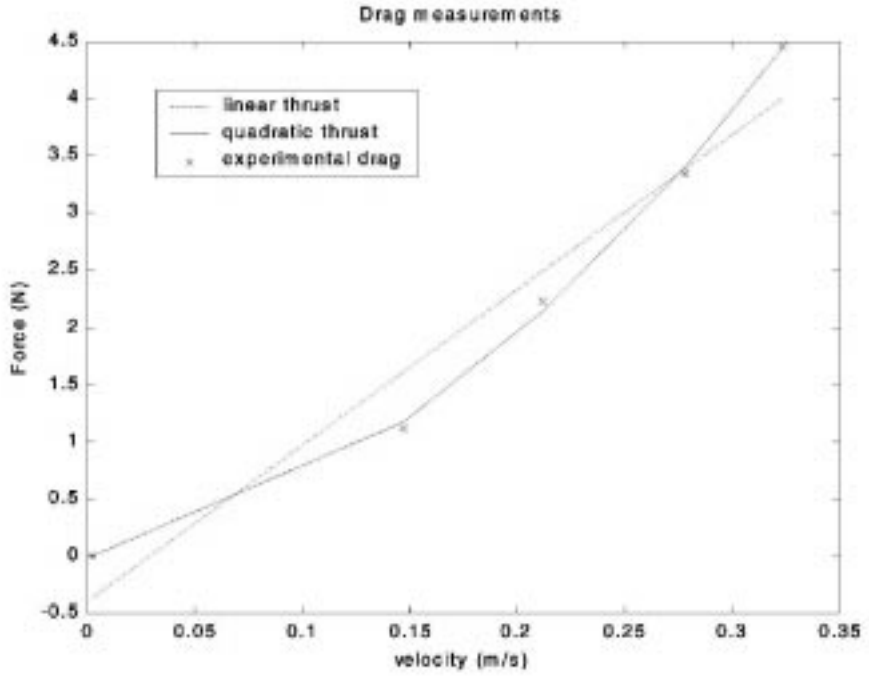

Fig. 16. Linear and quadratic polyfit curves used to determine thrust force.

Using the linear and quadratic polyfit curves allowed us to input velocities of the corresponding gait names and acquire respective thrust values. By using these thrust values, we created experimental thrust surfaces (Figs. 17-18). In addition, we created a theoretical surface (Fig. 19) using Ahlborn *et al.*'s equation and the given parameters. Our experimental surface (Fig. 20) was then graphed on the same intervals as Fig. 19. Calculations were made within the programs, but the equations for our experimental thrust force can be found if needed.

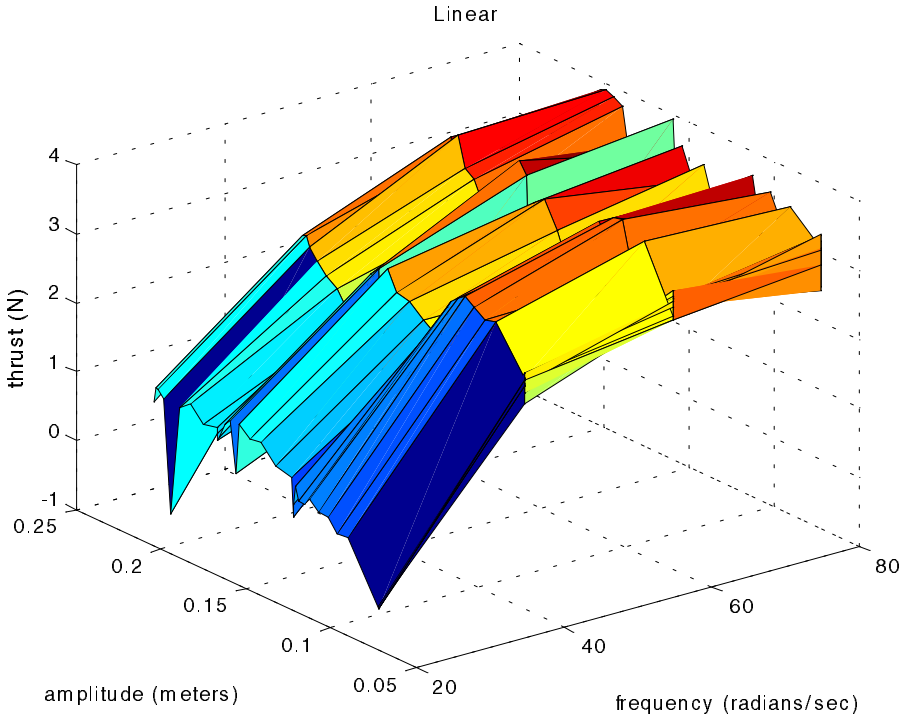

Fig. 17. Surface of linear fit.

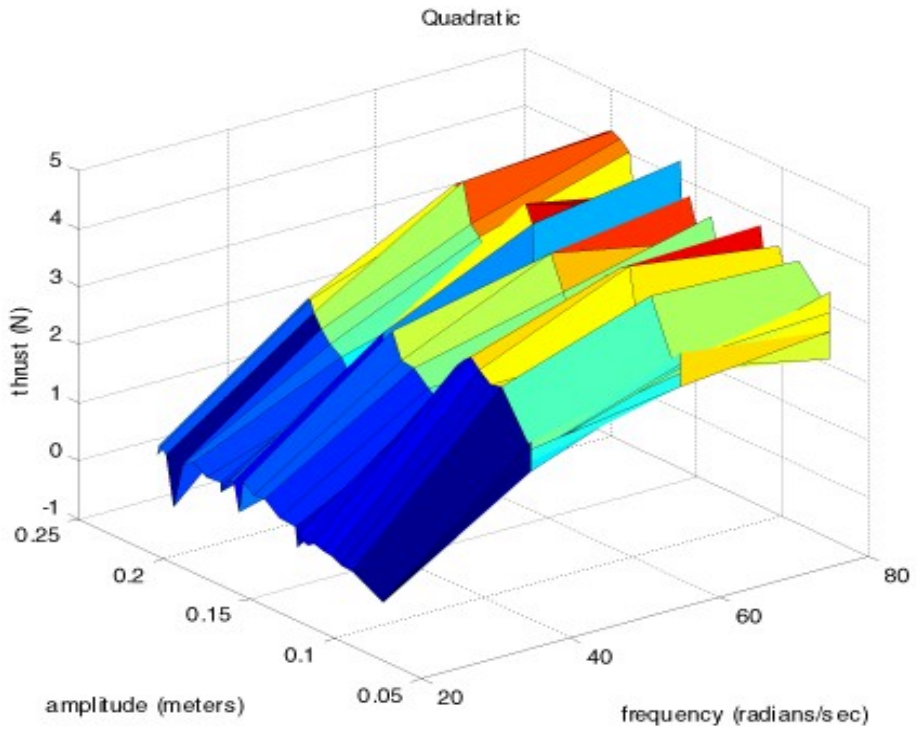

Fig. 18. Surface of Quadratic polyfit.

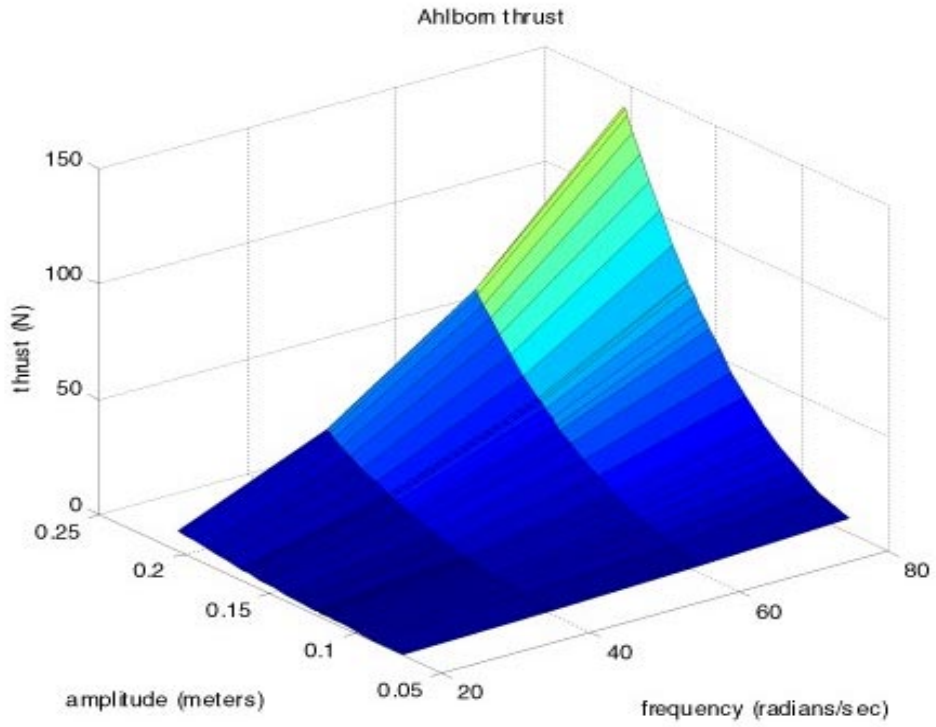

Fig. 19. Thrust predictions according to Ahlborn *et al.*

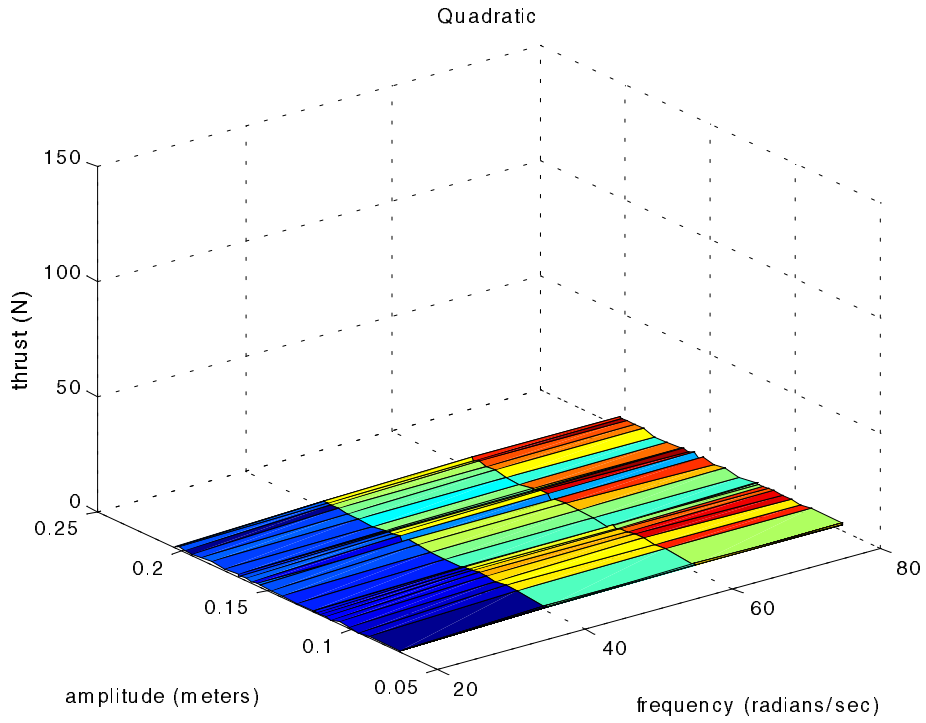

Fig. 20 Experimental thrust on the same axis.

Optimizing gaits

We created constraints where the velocity and efficiency were nonnegative and of equal importance. We matched the range of relative efficiency to that of the velocity, added the corresponding values, and found the maxima in Microsoft Excel 2000.

Chapter 4, Results

Optimizing velocity

Maxima over the entire surface were found at the following gaits:

–50P20W22 = 0.4202 meters/sec
–60P40W21 = 0.8532 meters/sec
–30P60W22 = 1.0312 meters/sec
–40P80W23 = 1.0440 meters/sec

Optimizing efficiency

Maxima over the entire surface were found at the following gaits:

–80P20W22 = 0.0056
–70P40W21 = 0.0113
–50P60W21 = 0.0139
–00P80W20 = 0.0105

Controlling thrust

It appeared that our fish has

$$F_x \propto f^{1/2} \tag{17}$$

as opposed to

$$F_x \propto f^{2} \tag{18}$$

as stated by Ahlborn *et. al.* (Fig. 18-19). Our experimental thrust force seemed directly proportional to the square root of the frequency. Thrust force of the robot appeared less than expected, as well.

Optimizing gaits

Where velocity and efficiency was of equal importance, the best motions were found at the following gaits:

–70P20W22
–60P40W21
–40P60W21
–30P80W20

The “best” gait was found at 40P60W21. It had a velocity of 0.9763 meters per second and an efficiency of 0.0139. The second, third, and fourth optimal gaits were at 30P60W21, 60P60W21, and 20P60W21, respectively (Tab. 1).

		tailfin amplitude (encoder ticks)				
		0	100	200	300	**MAX**
phase difference (degrees)	0	N/A	N/A	N/A	N/A	N/A
	10	1.5986	1.3641	1.7148	1.6450	1.7148
	20	1.6222	1.7515	1.5198	1.7037	1.7515
	30	1.5867	1.8494	1.5582	1.4022	1.8494
	40	1.6612	1.9363	1.3046	1.0889	1.9363
	50	1.2537	1.7281	1.0794	1.0077	1.7281
	60	1.4731	1.8082	1.1100	0.8670	1.8082
	70	1.6113	1.7924	0.9491	0.6593	1.7924
	80	1.5721	1.2510	0.7560	0.5145	1.5721
	90	1.3679	1.5043	0.6931	0.5198	1.5043
	MAX	1.6612	1.9363	1.7148	1.7037	1.9363

Table 1. Data used to find best gait; frequency at 6.0 rads/sec

Chapter 5, Discussion

Optimizing velocity

We were interested in discovering the inputs that yield the fastest gait. Data shows that velocity increased as the frequency increases, while the amplitudes varied, and as phase angles seemed to decrease. Initially, we did see that relationship where velocity and frequency increased (Figs. 6-9). At increased frequencies, we got more distortion and irregularity, but the same relationships are consistent. It appeared that the amplitudes would vary for the different frequencies of velocity. Optimal velocity was achieved when phase angles were in the 30, 40, 50, 60 values accompanied by high frequency and high amplitude. For future experiments, the 45-degree phase angle will be tested and analyzed. This may be the optimal phase angle according to previous unpublished work done with the older versions of the robot.

Optimizing efficiency

We were interested in discovering the inputs that yield the most efficient gait within the restrictions. Data showed that efficiency increased as the frequency appeared to increase, the amplitude decreased, and the phase angle decreased. The relation between relative efficiency and frequency must be interpreted with caution. As frequency increased, the overall efficiency rose. But then in Fig. 14,overall efficiency dropped. Within the parameters, the efficiency was the best at a frequency of 6.0 radians/sec (Figs. 10-14). Yet, there were huge drop-offs in the surfaces. We lost a lot of efficiency with a change of amplitude. Upon visual analysis, it appeared that would increase as frequency increased as long as the amplitude would decrease at the same time. We assumed that at high frequencies that the overall efficiency will decrease. The relationship with amplitudes here was difficult to interpret due to some randomness in the data. Changing the

phase angle varies the value for efficiency, almost unpredictably. Optimal efficiency may be found at a frequency at or near 6.0 radians/sec, with amplitude at or near 100 encoder ticks, and where phase angle is approaching 90 degrees.

With these results, we come closer to controlling the outputs that we want for a given gait. Efficiency and velocity differ where maxima were not found at the same gait. So by changing the parameters of the amplitude, frequency, and phase angle, we can achieve either optimal velocity or optimal efficiency. Further research will be done at different increased values of A_t and A_p. Further experiments will be performed on the latest model.

Controlling Thrust

Although we came to a different idea on thrust, our goal was not to disprove claims by Ahlborn *et al*. We simply used his findings as a guide. Both of our robots produced thrust by shedding counter-rotating vortices. However, our robot was allowed to "swim," while their apparatus was stationary. Our robot would have added mass effects and more forces acting on the tailfin, peduncle, and body than in the tail-flip apparatus. These additional forces are at times when the robot has not achieved a steady state velocity. Despite this, a real-time computer simulation of the robot was created after obtaining drag force calculations.

Despite the differences shown graphically, we believe that the equation was useful for our results. We may recalculate the steady state velocities. For some of the heavier weights, we may not achieve the most accurate velocity approximations due to the length of the tank. The relationship between amplitude and thrust force was not clear.

Optimizing gaits

Since the experimental thrust force is a function of velocity, we can assume that the optimal gaits at different frequencies will be equal. When thrust and efficiency are equally

important, we find the best motions at the same gaits. It is clear that efficiency made the difference. Optimization lowered the phase angles by ten degrees in some cases. We noticed that the data became increasingly unpredictable at the higher frequencies. Using Pareto optimization at varied constraints may give us several critical gaits for our robot.

Chapter 6, Conclusions

We have learned how to control our robot within certain parameters. Obviously, this robot was not as advanced a swimmer as a real fish. However, we believe our experiments have brought us a closer understanding of aquatic locomotion.

The use of Multiobjective Optimization found the best motion for our robot under a constraint. Taking a graduate course in linear programming and non-linear programming would make this easier to model. An introductory course in fluid dynamics would also help.

Currently, we plan to modify the transmission, anodize the body, and redo experiments. We may try experiments with various tailfin shapes, i.e. lunate, crescent moon shaped. The use of different tailfin shapes moving to a larger aquarium may prove to be advantageous for data accuracy. More degrees of freedom will be added in future experiments. The velocity, efficiency, and drag experiments will be repeated with a modified version of the robot. Additionally, calculations of absolute efficiency will be made.

This research has helped improve our current understanding of robotic swimming. We can control the velocity, efficiency, and thrust force produced by the robot within certain parameters. Hopefully, many future applications in military defense, satellite communication, subterranean exploration, “fishing”, and others will become available with the advent of a free-swimming robotic fish.

List of symbols

F_x	thrust force
π	pi (=3.14159 . . .)
K	water entrainment constant of 40
ρ	density of water (approx. 1000 kg m^3)
h	submerged height of the tailfin
A	amplitude of tail tip deflection
A_p	amplitude of the peduncle
A_t	amplitude of the tailfin
θ	joint angle
θ_p	joint angle of the peduncle
θ_t	joint angle of the tailfin
f	frequency
ϕ	phase difference angle
ϕ_p	phase angle of the peduncle
ϕ_t	phase angle of the tailfin
ω	angular velocity
##P	phase angle
##W	frequency
fps#	forward velocity
T	thrust force
D	drag force
hmax	maximum deflection of the peduncle and tailfin
hmin	minimum deflection of the peduncle and tailfin
joutp	actual encoder angles of the peduncle
joutt	actual encoder angles of the tailfin
lp	length of the peduncle
lt	length of the tailfin

Bibliography

Ahlborn, B., Chapman, S., Stafford, R., Blake, R. W. and Harper, D. G. (1997) Experimental simulation of the thrust phases of fast-start swimming of fish. *J. exp. Biol.* **200**, 2301-2312.

Ahlborn, B., Harper, D. G., Blake, R. W., Ahlborn, D. and Cam, M. (1991) Fish without footprints. *J. exp. Biol.* **148**, 521-533.

Eschenauer, H.A., J. Koski, and A. Osyczka (1986) *Multicriteria Design Optimization : Procedures and Applications.* Springer-Verlag, New York.

Muller, U. K., Van Den Huevel, B. L. E., Stamhuis, E. J. and Videler, J. J. (1997) Fish foot prints. *J. exp. Biol.* **200**, 2893-2906.

Hussaini, Y. M., (1997) *Collected Papers of Sir James Lighthill.* Oxford: Oxford University Press.

Lewis, F. L., (1992) Applied Optimal Control and Estimation, Prentice-Hall.

Lighthill, M. J. (1970) Aquatic animal propulsion of high hydromechanical efficiency. *J. Fluid Mech.* **44**, 265-301.

O'Neill, M. E. and Chorlton, F. (1986) *Ideal and Incompressible Fluid Dynamics*. Ellis Horwood Limited. Chichester

Shapiro, A. H., (1961) *Shape and Flow: The fluid dynamics of drag*. Anchor Books, Doubleday & Company, Inc. Garden City, New York.

Triantafyllou, M. S. and Streitlien, K. (1995) Force and moment on a Joukowski profile in the presence of point vortices. *AIAA Jour.* **33**, 603-610.

Weihs, D. (1989) Design features and mechanics of axial locomotion in fish. *Amer. Zool.* **29**, 151-160.